Journal of Alloys and Compounds 1040 (2025) 182887

Contents lists available at ScienceDirect

Journal of Alloys and Compounds

journal homepage: www.elsevier.com/locate/jalcom

Research article

Griffiths phase and magnetocaloric effect in ferromagnetic $La_{0.7}Sr_{0.3}Mn_{0.9}Fe_{0.1-x}Zn_xO_3$ ($x = 0.05$, 0.075 and 0.1)

Z.Y. Seidov [a,g], I.V. Yatsyk [b], A.V. Shestakov [c], A.S. Ovchinnikov [d], F.G. Vagizov [e], V.A. Shustov [b], A.G. Badelin [f], V.K. Karpasyuk [f], M.J. Najafzade [a], I.N. Ibrahimov [a], H.-A. Krug von Nidda [g,*], R.M. Eremina [b]

[a] Institute of Physics, Ministry of Science and Education, AZ-1073 Baku, Azerbaijan
[b] Zavoisky Physical-Technical Institute, Federal Research "Kazan Scientific Center of RAS", 420029 Kazan, Russia
[c] Prokhorov General Physics Institute of the Russian Academy of Sciences, 119991 Moscow, Russia
[d] Institute of Natural Sciences and Mathematics, Ural Federal University, 620002 Ekaterinburg, Russia
[e] Institute of Physics, Kazan Federal University, 420008 Kazan, Russia
[f] Astrakhan State University, 414056 Astrakhan, Russia
[g] Experimental Physics V, Center for Electronic Correlations and Magnetism, Institute of Physics, University of Augsburg, D-86135 Augsburg, Germany

ARTICLE INFO

Keywords:
Manganites
Griffiths phase
Magnetocaloric effect
EPR
Magnetic susceptibilities
Mössbauer spectroscopy

ABSTRACT

The polycrystalline $La_{0.7}Sr_{0.3}Mn_{0.9}Fe_{0.1-x}Zn_xO_3$ (x= 0.05, 0.075 and 0.1) have been investigated by means of electron spin resonance (ESR), magnetic susceptibility, magnetization, and Mössbauer measurements. Mössbauer studies for $x = 0.05$ indicate that Fe in these compounds is in the trivalent high-spin state. All compounds exhibits a paramagnetic to ferromagnetic transition at the Curie temperature T_C. The Curie temperature T_C decreases on increasing Zn content according to 278, 193 and 166 K for $x = 0.05$, 0.075 and 0.1, respectively. The existence of a Griffiths like phase is experimentally detected by means of magnetic susceptibility and ESR measurements and corroborated by theoretical modeling. We also observed a magnetocaloric effect with a maximum magnetic entropy change ($|\Delta S_M^{max}|$) value occurring close to the Curie temperature T_C, corresponding to $|\Delta S_M^{max}|$ = 2.9, 2.6 and 2.68 J/(kg K) under magnetic field change (ΔH) of 50 kOe for x = 0.05, 0.075 and 0.1, respectively. The relative cooling power values were found to vary between 0.25 and 0.31 kJ/kg.

1. Introduction

Manganites of the general composition $R_{1-x}A_xMnO_3$, with trivalent rare-earth R and divalent alkali-earth A ions sharing the A-site of the perovskite structure, are of high interest for application in spintronics due to their peculiar thermodynamic and transport properties [1–8]. In these compounds the strong coupling between electronic charge, orbital and spin with the crystal lattice gives rise to complex magnetic phase diagrams comprising e.g. charge- and orbital order, metal–insulator transitions, colossal magnetoresistance (CMR) effect, and phase separation [9,10]. Transitions from antiferromagnetic (AFM) insulating to ferromagnetic (FM) metallic phases mainly result from the interplay between double-exchange (DE: Mn^{3+}–O^{2-}–Mn^{4+}) and super-exchange (SE: Mn^{3+}–O^{2-}–Mn^{3+} or Mn^{4+}–O^{2-}–Mn^{4+}) interactions [1,11,12]. But influence from e.g. crystal electric field, Jahn–Teller effect, and Dzyaloshinskii–Moriya interaction are decisive to understand the details of the phase diagrams. Additionally, recent researches have indicated that perovskite oxides including mixed-valence manganites can be considered as promising candidates for magnetic refrigeration [13–23], thus opening up new possibilities for their potential applications. The magnetic refrigeration has attracted much attention due to its potential impact on energy savings and environmental friendliness compared with gas compression refrigeration technologies [24,25].

While substitution on the A site keeps the manganese lattice intact, but partially changes the valence of the manganese ions and influences the local lattice distortions, co-substitution of other magnetic or non-magnetic ions on the manganese site introduces disorder. Non magnetic Zn^{2+} changes Mn^{3+} into Mn^{4+}, but also locally interrupts the magnetic structure and hinders electronic transport, because it cannot change its valency. Magnetic Fe^{3+} does not change Mn^{3+} valency, but provides a larger local moment. Such co-substitution is applied to fine tune the electronic properties of manganites. For example our recent studies of the magnetic properties of $La_{0.83}Sr_{0.17}Mn_{0.9}Fe_{0.1-x}Zn_xO_3$ (x=0, 0.05) [26] at the verge of the FM metallic regime, showed that the compound with concentration $x = 0.05$ exhibits features characteristic

* Corresponding author.
E-mail address: hans-albrecht.krug@physik.uni-augsburg.de (H.-A.K.v. Nidda).

https://doi.org/10.1016/j.jallcom.2025.182887
Received 18 December 2024; Received in revised form 14 July 2025; Accepted 7 August 2025
Available online 19 August 2025

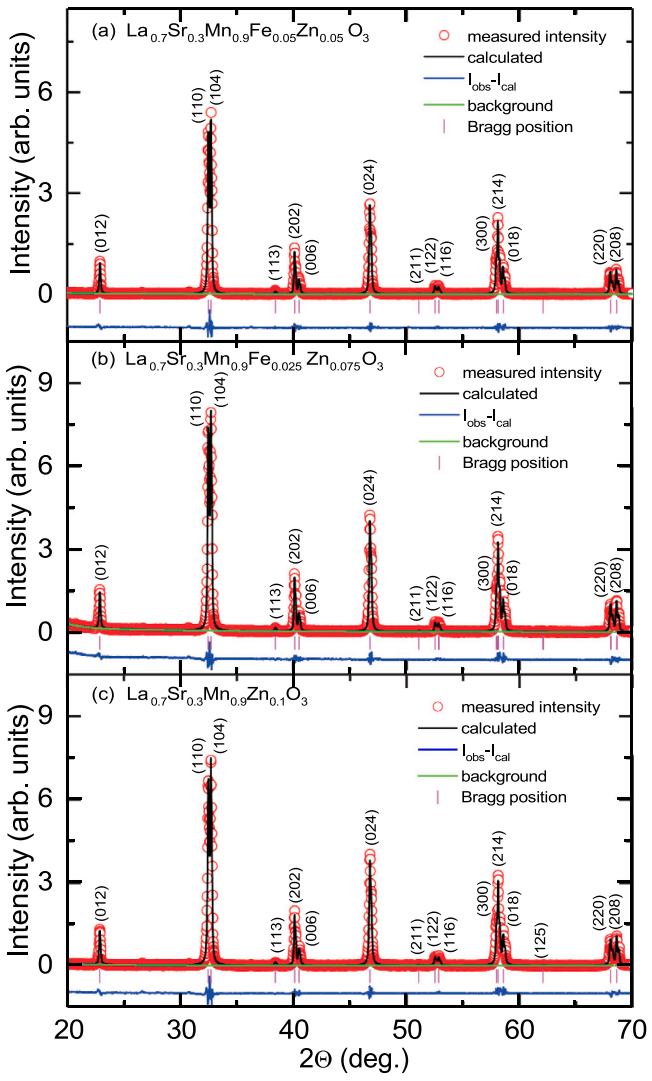

Fig. 1. X-ray diffraction patterns of $La_{0.7}Sr_{0.3}Mn_{0.9}Fe_{0.1-x}Zn_xO_3$ ceramic samples at room temperature for (a) $x = 0.05$, (b) $x = 0.075$ and (c) $x = 0.1$.

of a Griffiths-like phase [27–30], i.e. the co-existence of FM clusters and paramagnetic (PM) phase within a temperature regime $T_C \leq T \leq T_G$ above the onset of FM order at the Curie temperature T_C. But for $x = 0$, the onset of magnetic order shifts to lower temperature and the Griffiths regime is suppressed, i.e. the balance of disorder and AFM Fe^{3+}–O^{2-}–Mn^{3+} exchange is important.

In this article, we focus on a DE dominated compound with 30% Sr substitution, i.e. deeply in the FM metallic regime. Again we find characteristics of a Griffiths phase (GP) in polycrystalline $La_{0.7}Sr_{0.3}Mn_{0.9}Fe_{0.1-x}Zn_xO_3$ (x=0.05, 0.075 and 0.1) via dc susceptibility and ESR measurements. In addition we investigate the magnetocaloric effect dependent on the Fe:Zn ratio. Fe-57 Mössbauer spectroscopy is applied for determination of valence and spin state of the iron ions.

2. Sample preparaton, characterization and experimental methods

Polycrystalline samples of $La^{3+}_{0.7}Sr^{2+}_{0.3}Mn^{3+}_{0.6-x}Mn^{4+}_{0.3+x}Fe^{3+}_{0.1-x}Zn^{2+}_{x}O^{2-}_{3}$ with zinc content $x = 0.05$, 0.075, 0.1 were synthesized by solid-phase reactions in air using strontium carbonate ($SrCO_3$-99.9%), oxides of lanthanum (La_2O_3-99.9%), manganese (Mn_2O_3-99.9%), iron (Fe_2O_3-99.9%), and zinc (ZnO-99.9%) as starting materials. These included

Table 1
Crystallographic data for $La_{0.7}Sr_{0.3}Mn_{0.9}Fe_{0.1-x}Zn_xO_3$ (x=0.05, 0.075, 0.1).

Sample (x)	x=0.05	x=0.075	x= 0.1
Space group	$R\bar{3}c$	$R\bar{3}c$	$R\bar{3}c$
a (Å)	5.5105(1)	5.509(1)	5.5082(1)
c (Å)	13.3571(3)	13.3535(3)	13.3498(3)
V (Å^3)	351.259979	350.971973	350.772591
La/Sr (6a)			
x	0	0	0
y	0	0	0
z	0.25000	0.25000	0.25000
Mn1/Mn2 (6b)			
x	0	0	0
y	0	0	0
z	0	0	0
Fe/Zn (6b)			
x	0	0	0
y	0	0	0
z	0	0	0
O (18e)			
x	0.45753	0.45669	0.45543
y	0	0	0
z	0.25000	0.25000	0.25000
Distance Mn–O (Å)	1.95557(3)	1.9556(3)	1.95608(3)
Ang. Mn–O–Mn (deg.)	166.2532(0)	165.9846(6)	165.5786(0)

two grinding stages in a ball mill with ethanol addition, followed by a preliminary heat treatment at 1273 K for 4 h. The final sintering was performed in air at 1473 K for 10 h, and the samples were then cooled together with the furnace. To ensure stoichiometric oxygen content ($\delta = 0$), the samples were annealed at 1223 K under an oxygen partial pressure $p_{O_2} = 10^{-1}$ Pa for 96 h, based on the conditions outlined in Ref. [31].

The phase composition and unit cell parameters were determined via powder X-ray diffraction at room temperature using a Shimadzu XRD-7000 diffractometer with Cu K_α radiation. X-ray diffraction analysis of the synthesized manganites confirmed that all compounds were single-phase, with a structure corresponding to the $R\bar{3}c$ space group. These results of our X-ray investigations are in agreement with earlier work on $La_{0.7}Sr_{0.3}MnO_3$, $La_{0.7}Sr_{0.3}Mn_{1-x}Fe_xO_3$, $La_{0.67}Sr_{0.33}Mn_{1-x}Fe_xO_3$ ($0 \leq x \leq 0.15$), $La_{0.6}Sr_{0.4}Mn_{1-x}Fe_xO_3$ ($0 \leq x \leq 0.3$) and $La_{0.8}Sr_{0.2}Mn_{1-x}Fe_xO_3$ ($0 \leq x \leq 0.15$) polycrystalline and nanocrystalline powders [7,8,32–40]. The diffraction patterns of the samples are presented in Fig. 1(a, b, c). The unit cell parameters, as shown in Table 1, were determined and refined using the Maud-v2.94 software package [41,42].

Mössbauer measurements were carried out at several temperatures between 4.2 K and room temperature (RT) on a conventional constant-acceleration spectrometer (WissEl) that utilizes a Co-57 source in Rh-matrix at room temperature. An iron foil of 7 μm thickness was used to calibrate the spectrometer and the zero velocity is taken as the centroid of its room temperature Mössbauer spectrum.

The Mössbauer spectra of $La_{0.7}Sr_{0.3}Mn_{0.9}Fe_{0.05}Zn_{0.05}O_3$ at different temperatures are shown in Fig. 2. At room temperature (lower frame), the Mössbauer spectrum consists of a slightly asymmetric doublet with a distribution of isomer (IS) and quadrupole shifts (QS). In the insets of Fig. 2 the distribution functions of the Mössbauer parameters are given. They were restored by processing the experimental spectra with the SpectrRelax software [43]. At RT the distribution function of isomer shifts shows the presence of two well defined centers of iron ions with an area ratio close to 1:5. As it is known, the isomer shift reflects the density of s-electrons in the iron nucleus, and it is sensitive to the oxidation state of iron and the coordination number. The average values of the IS and QS of Fe nuclei in the studied sample are found as 0.35 mm/s and 0.19 mm/s, respectively which are in good agreement with the previously reported Mössbauer data for $La_{0.83}Sr_{0.17}Mn_{0.9}Fe_{0.05}Zn_{0.05}O_3$ and $La_{0.81}Sr_{0.19}Mn_{0.9}Fe_{0.05}Zn_{0.05}O_3$ [26,44]. These values of the IS and QS are typical for Fe^{3+} ions in the

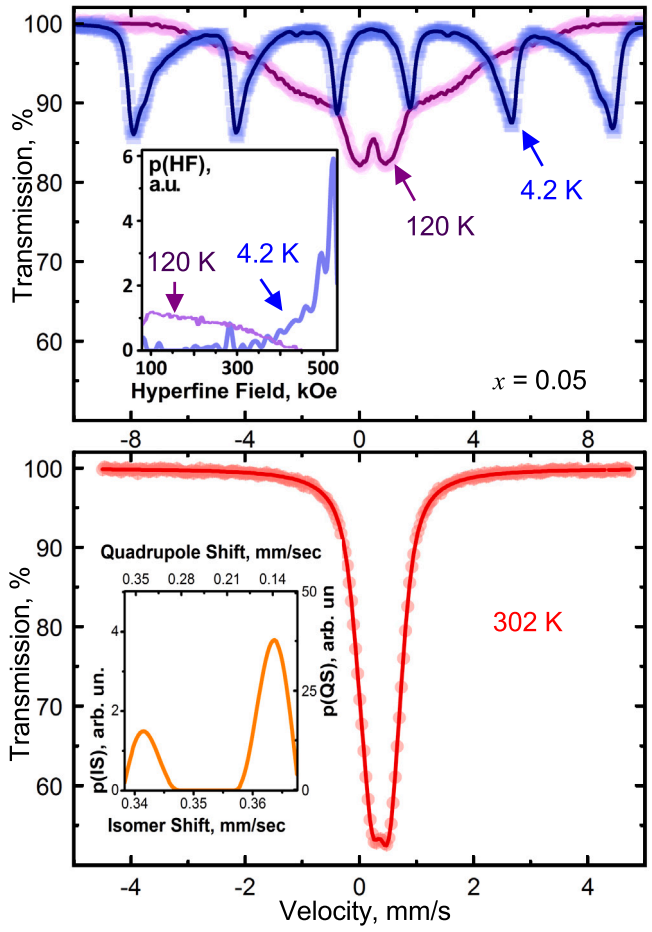

Fig. 2. Mössbauer spectra of the sample $La_{0.7}Sr_{0.3}Mn_{0.9}Fe_{0.05}Zn_{0.05}O_3$ at temperatures 4.2 K, 120 K, and 302 K. Insets show the reconstructed distribution functions of isomer shift (302 K) and hyperfine field (4.2 K, 120 K).

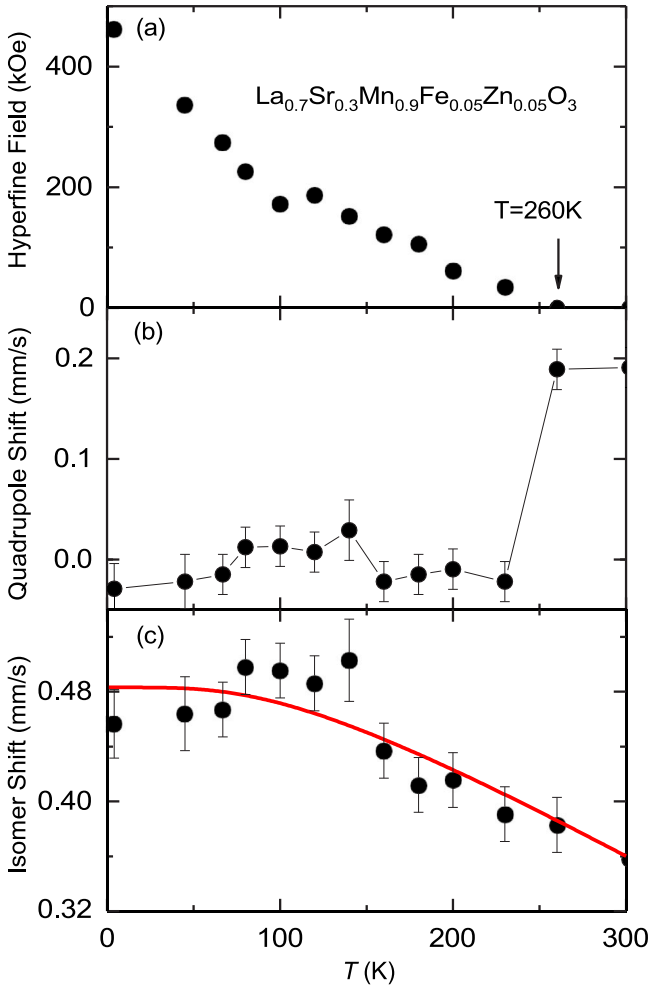

Fig. 3. Temperature dependence of Mössbauer parameters of ^{57}Fe in $La_{0.7}Sr_{0.3}Mn_{0.9}Fe_{0.05}Zn_{0.05}O_3$: (a) the average hyperfine magnetic field on the iron nuclei. (b) the average quadrupole shift, ϵ, (c) the average isomer shift, δ. The red solid line represents the best fitting in Debye approximation.

high spin state, ($t_{2g}^3 e_g^2$) [45,46]. Also the hyperfine fields determined at low temperature are in good agreement with the data reported in the literature for similar compounds [26,47,48].

The substitution of La by a divalent cation, Sr, results partly in a change of the Mn valence from 3+ to 4+ [47], so that a part of Mn^{3+} is transformed into Mn^{4+}. Therefore it makes sense to check the presence of Fe^{4+} absorption lines in the Mössbauer spectra at room temperature. The absorption lines Fe^{4+} ions are located in the region of low velocities down to −0.25 mm/s. As can be seen from the distribution function for the isomer shift in Fig. 2, in this velocity region, the features due to Fe^{4+} ions are not observed. Probably, the preferable substitution of Fe^{3+} ions for Mn^{3+} ions is due to the identical ion size of these elements in the high-spin state. As the temperature decreases, the Mössbauer spectra change noticeably. As can be seen from Fig. 2 (upper frame), at temperatures close to 140–120 K, the Mössbauer spectrum takes the form of a relaxation spectrum with a wide distribution of hyperfine magnetic fields up to 300 kOe (and more), and then, in the temperature range of liquid helium, the Mössbauer spectra are transformed into magnetic sextets (Fig. 2, upper frame). At a temperature of 4.2 K, a noticeable peak is observed in the distribution of hyperfine fields at a value of 520 kOe and an extended tail towards low fields (inset in Fig. 2, upper frame).

The temperature dependence of the mean hyperfine field is given in Fig. 3(a). According to the Mössbauer measurements, magnetic ordering of the iron ions is achieved at a temperature of 260 K for $La_{0.7}Sr_{0.3}Mn_{0.9}Fe_{0.05}Zn_{0.05}O_3$. The changes observed in the temperature dependence of the mean quadrupole shift, ϵ, also indicate the magnetic ordering of the iron ions (cf. Fig. 3(b)). When an ion is in the paramagnetic state, the splitting ΔE_Q between the lines of the quadrupole doublet is determined by the product of the electric field gradient (EFG) q at the nucleus and the nuclear quadrupole moment Q, i.e. $\Delta E_Q \approx 2\epsilon = e^2qQ/2$. In the case of magnetic ordering of resonant atoms and the appearance of a hyperfine magnetic field on the nucleus oriented with respect to the direction of the main axis of the quadrupole interaction tensor at some angle θ, the quadrupole shift ϵ is determined by the expression: $\epsilon = e^2qQ\cdot(3\cos^2\theta - 1)/8$. Under a random orientation of the hyperfine magnetic field directions this angle theta will be different for different atoms. The sharp decrease of the quadrupole shift observed in the region of the magnetic ordering temperature is probably due to the appearance of a hyperfine magnetic field on the nucleus at some angle to the direction of the EFG and the averaging of the quadrupole angular factor over all possible values of theta. The temperature dependence of the average isomer shift of iron ions presented in Fig. 3(c), is mainly determined by the second order Doppler effect. Its value decreases monotonically with increasing temperature. In the figure, the solid line represents the best fit in the Debye approximation (Θ_D= 432 ± 16 K) to the experimental values of the average isomer shift.

Magnetization measurements were performed using a superconducting quantum interference device (SQUID) magnetometer MPMS5 (Quantum Design) in magnetic fields up to $H \leq 50$ kOe for the temperature regime $1.8 \leq T \leq 400$ K. ESR measurements have been

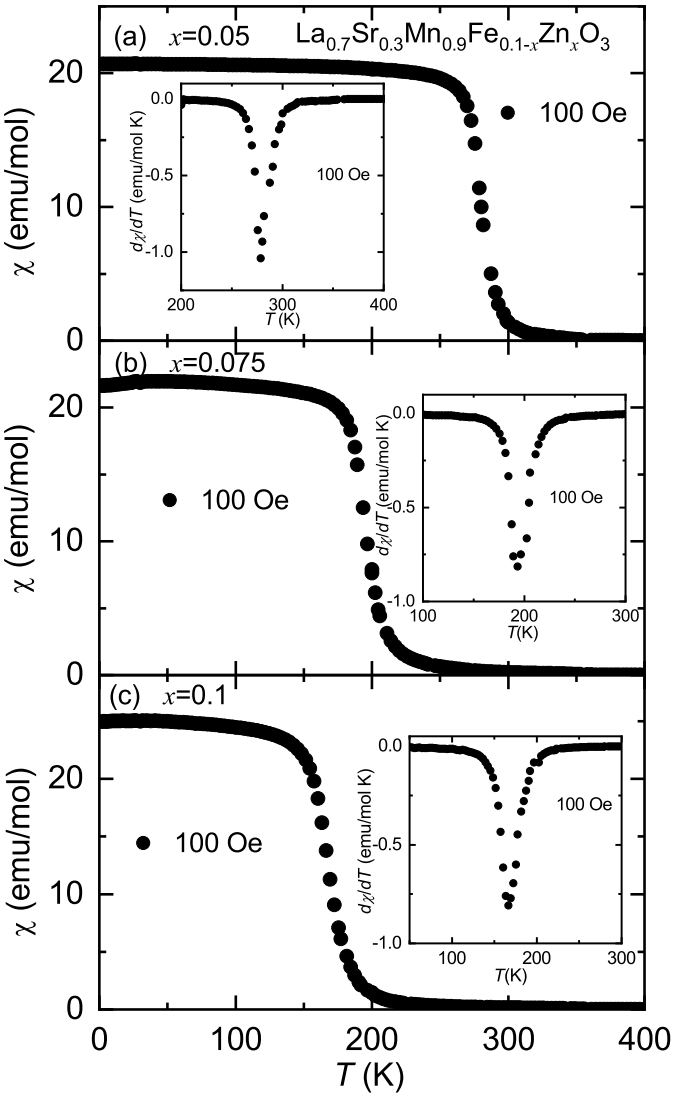

Fig. 4. Temperature dependence of dc magnetic susceptibility at H = 100 Oe in $La_{0.7}Sr_{0.3}Mn_{0.9}Fe_{0.1-x}Zn_xO_3$ (x=0.05, 0.075, 0.1). Inset: The derivative of magnetic susceptibility $d\chi(T)/dT$ as a function of temperature.

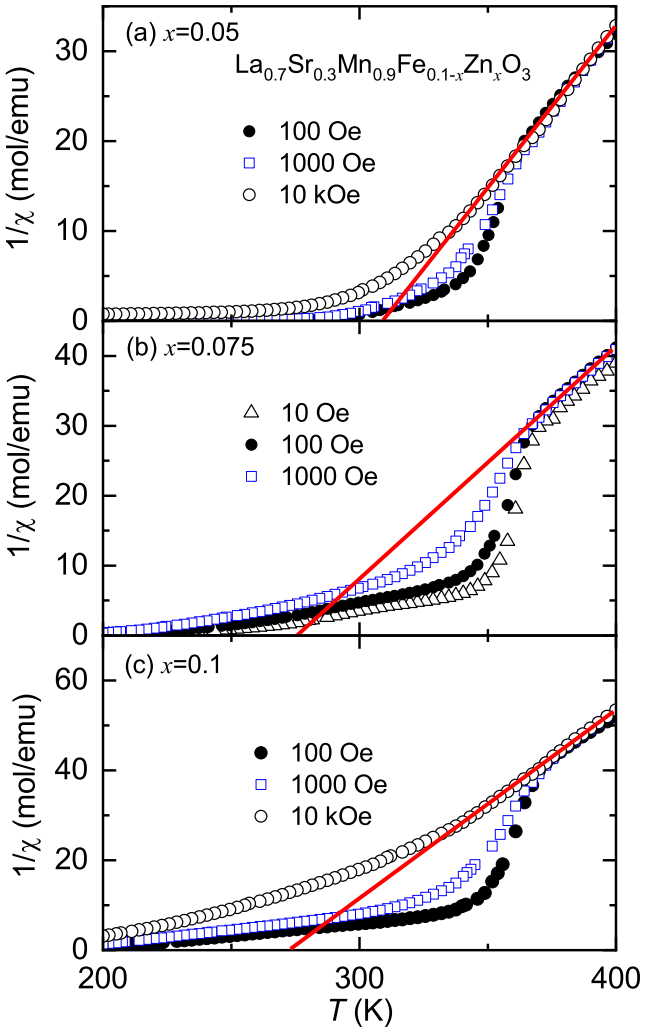

Fig. 5. Temperature dependence of dc inverse magnetic susceptibility in $La_{0.7}Sr_{0.3}Mn_{0.9}Fe_{0.1-x}Zn_xO_3$ (x=0.05, 0.075, 0.1) at 10 Oe, 100 Oe, 1000 Oe and 10 kOe. The solid line indicates a fit by a Curie–Weiss law.

performed using a BRUKER EMXplus spectrometer working at X-band frequency (9.4 GHz) and equipped with a nitrogen gas-flow cryostat. Due to the lock-in technique with field modulation, the field derivative of the absorbed microwave power (dP/dH) is recorded as a function of the externally applied field.

3. Results and discussion

3.1. Magnetization study

Figs. 4 and 5 show the temperature dependence of the magnetic susceptibility and its inverse for x=0.05, 0.075, and 0.1, respectively. The Curie temperature T_C, identified by the minimum of $d\chi/dT$ in the χ vs T curve (see Insets in Fig. 4), amounts to $T_C(x = 0.05)$ = 278 K, $T_C(x = 0.075)$ = 193 K, and $T_C(x = 0.1)$ = 166 K, respectively (cf. Table 2). The effective moments determined from the CW law as $\mu_{eff}(x = 0.05) = 4.73\ \mu_B$, $\mu_{eff}(x = 0.075) = 4.88\ \mu_B$, and $\mu_{eff}(x = 0.1) = 4.354\ \mu_B$ are significantly enhanced compared to the theoretical values of 4.494 $\mu_B(x = 0.05)$, 4.421 $\mu_B(x = 0.075)$, and 4.243 $\mu_B(x = 0.1)$, calculated from the square root of the sum of squared ionic moments of Mn^{3+} (S = 2), Mn^{4+} (S = 3/2), and Fe^{3+} (S = 5/2) weighted by the corresponding stoichiometric factors and using the spin-only g-value g = 2 [49].

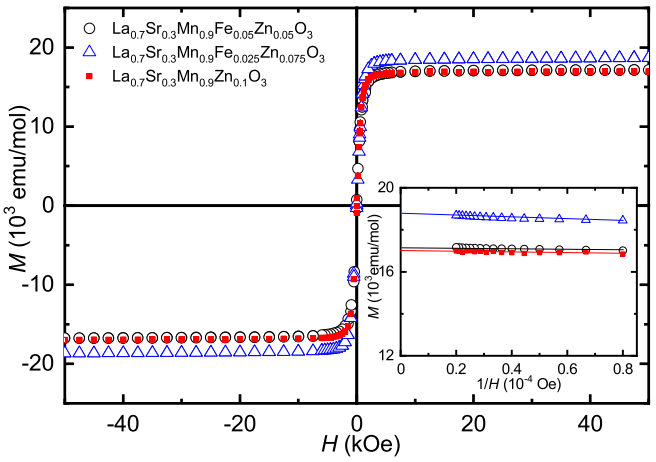

Fig. 6. Magnetization as a function of external field in $La_{0.7}Sr_{0.3}Mn_{0.9}Fe_{0.05}Zn_{0.05}O_3$, $La_{0.7}Sr_{0.3}Mn_{0.9}Fe_{0.025}Zn_{0.075}O_3$ and $La_{0.7}Sr_{0.3}Mn_{0.9}Zn_{0.1}O_3$ at 2 K. Inset: magnetization as function of inverse magnetic field to determine the saturation magnetization.

Table 2
Magnetization M at 2 K (in μ_B per formula unit), paramagnetic Curie temperature Θ_{CW}(K), magnetic ordering temperature T_C, effective paramagnetic moment $\mu_{eff}(\mu_B/\text{f.u.})$ and g_0, A_0 values of the scaling parameters in $La_{0.7}Sr_{0.3}Mn_{0.9}Fe_{0.1-x}Zn_xO_3$ (x=0.05, 0.075, 0.1).

x	$M_S(\mu_B/\text{f.u.})$	Θ_{CW} (K)	T_C (K)	$\mu_{eff}(\mu_B/\text{f.u.})$	g_0	A_0
x=0.05	3.074	309	278	4.730	0.526	0.030
x=0.075	3.371	276	193	4.887	0.467	0.019
x=0.1	3.044	273	166	4.354	0.595	0.018

Fig. 6 shows the magnetization of all three compounds under consideration as a function of magnetic field at 2 K. The magnetization for $x = 0.05$, $x = 0.075$, and $x = 0.1$ reveals practically no hysteresis and immediately reaches the full saturation value at weak external fields. The saturation magnetization (M_S) in all three compounds was obtained from a linear extrapolation of the high-field data [26,50] down to $1/H = 0$ as illustrated in the inset of Fig. 6 and the values of $M_S(T = 2\,\text{K})$ are deduced to be 3.074 μ_B, 3.371 μ_B, and 3.044 μ_B, respectively. Assuming all moments aligned parallel (or Fe moments antiparallel to Mn moments) this has to be compared to the theoretical values 3.5 (3.0) μ_B, 3.35 (3.1) μ_B, and 3.2 μ_B for $x = 0.05$, 0.075, and 0.1, respectively. This means that in case of 2.5% Fe content, the magnetic moments of iron prefer a parallel alignment to the ferromagnetic manganese lattice, but favor an antiparallel alignment already for 5% Fe.

3.2. Griffiths phase

Regarding the temperature dependence of the inverse susceptibilities depicted in Fig. 5 for different external fields, an anomalous downward deviation from the linear Curie–Weiss law shows up below $T_G \sim 364$ K, i.e. already significantly above T_C [26,44]. This deviation is the larger the lower the external field, but vanishes for high fields. Such behavior is typical for a Griffiths phase [49,51–57], due to FM clusters coexisting with the paramagnetic (PM) matrix. While the magnetization of the PM matrix increases linearly on increasing magnetic field H [26,44,51,56,57], the contribution of the FM clusters saturates already in small fields. Thus, at sufficiently high magnetic field the PM contribution dominates over the FM one. This observation corroborates the general tendency for FM cluster formation in the PM phase in these compounds.

The emergence of the Griffiths phase leads to the new scaling relation [58] near T_c for the magnetization measured as a function of the reduced temperature difference $t = |T - T_C|/T_C$ and the dimensionless magnetic field $h = \mu_B H/k_B T_C$

$$\frac{M(t,h)}{\mu} = -g_0 \text{Im}\left\{\exp\left[i\frac{A(t)}{2h}\right] E_1\left[\frac{A(t)}{\pi} + i\frac{A(t)}{2h}\right]\right\}. \quad (1)$$

Here, $E_1(z) = \int_z^\infty dx\, e^{-x}/x$, where $\text{Arg}(z) < \pi$ is the exponential integral, and μ is the magnetic moment of individual spins. The function $A(t)$ specifies the probability p_r that a randomly chosen site belongs to a large cluster of r spins, $p_r \sim \exp[-A(t)r]$ [59]. It has the form $A(t) = A_0 t^{2-\beta_r}$ with a constant A_0 and β_r is the critical exponent of the dilute system. According to Ref. [60], the estimation $\beta_r = 2\beta$ may be taken, where β is the critical exponent of the order parameter for the pure ferromagnet, i.e. $\beta \approx 0.36$ for the 3D Heisenberg model. The constant g_0 is related with the density of Lee–Yang zeros of the grand partition function [59,61,62]. The analysis of experimental data for magnetization in manganites and dichalcogenides intercalated by transition metal ions with the help of the scaling law (Eq. (1)) has demonstrated its effectiveness to establish the presence of a Griffiths phase [58,63].

Fig. 7 illustrates a comparison between the theoretically predicted universal scaling function and the experimental measurements at different magnetic fields. To determine the optimal parameters g_0 and A_0 from Eq. (1), the experimental magnetization for a magnetic field of 1000 Oe is taken as a function of the dimensionless temperature t in the paramagnetic region and then these data are fitted using Eq. (1). Taking into account that this form can be expanded near $A = 0$ in the critical region, the following expression becomes more convenient for fitting

$$\frac{M(t,h)}{\mu} = -g_0 \exp\left[-\frac{A(t)}{\pi}\right] \text{Im}\left\{\exp\left[i\frac{A(t)}{2h}\right] E_1\left[i\frac{A(t)}{2h}\right]\right\}. \quad (2)$$

The parameters obtained from this procedure are presented in Table 2 and are then used without modification to verify the scaling form for other values of magnetic fields. The parameters g_0 and A_0 were determined with an accuracy of three decimal places.

The scaling function itself can be approximated by [58]

$$\frac{M(t,h)}{\mu} \exp\left[+\frac{A(t)}{\pi}\right] \approx f\left[\frac{A(t)}{h}\right], \quad (3)$$

which is valid for small h and $A(t)$, but for the finite ratio $A(t)/h$. Here,

$$f(x) = -g_0 \text{Im}\left[\exp(ix/2)\, E_1(ix/2)\right]. \quad (4)$$

Apparently, the collapsed data for the magnetization are in line with those predicted by the Griffiths model.

To further identify the presence of the Griffiths phase, we performed electron spin resonance measurements on the three compounds. Due to its sensitivity to the local environment, ESR allows to distinguish signals from PM and FM regions. Hence, ESR has been already applied previously to identify the existence of Griffiths phases in several manganites [26,51,57,64–67].

The typical evolution of the ESR spectra on decreasing temperature from the PM into the FM state is shown for the sample with Zn concentration $x = 0.075$ in Fig. 8. Above $T \geq 360$ K in the purely PM regime only a single resonance line shows up. The g value $g = 1.96(1)$, which is found slightly below the spin-only value of 2, is usually observed for Mn^{3+} in octahedral ligand field. But on decreasing temperatures, a second peak splits from the main resonance, shifts to lower fields and gains intensity.

Both peaks coexist down to 200 K, indicating the coexistence of two different magnetic phases. Below $T = 200$ K, both peaks merge into a single resonance line, which further moves to lower magnetic fields. In Fig. 8, at $T < 200$ K, one can see that the sample has undergone the PM–FM phase transition and only the ferromagnetic resonance (FMR) line remains. Thus one recognizes that the temperature regime of coexisting ESR signals resembles the GP regime derived from the susceptibility data.

For the compounds $x = 0.05$ (from 350 K down to 290 K) and $x = 0.1$ (from 350 K down to 180 K) we also observed the splitting into two peaks, indicating the coexistence of two different magnetic phases, until they merge again into a single ferromagnetic resonance at lower temperatures $T < T_C$.

The full temperature dependences of the resonance fields H_{res} and linewidth data, obtained by fitting the ESR signal by the field derivative of two Lorentzians, are summarized in Fig. 9. The splitting of the resonance fields in $La_{0.7}Sr_{0.3}Mn_{0.9}Fe_{0.1-x}Zn_xO_3$ (x=0.05, 0.075 and 0.1) is characteristic of the coexistence of magnetic phases. The solid and open symbols in Fig. 9(a) depict the temperature dependence of the resonance fields for PM and FM peak, respectively. The position of the PM peak remains almost unchanged at a magnetic field of $H = 3.43$ kOe showing only a weak temperature dependence. At about 360 K (for $x = 0.1$ at slightly higher temperature) the FMR line separates from the PM one and shifts gradually to lower fields down to about 3 kOe, and further on crossing T_C where it merges again with the main resonance, which itself shifts to lower magnetic fields around the magnetic phase transition. Above the Curie temperature T_C, the linewidth of the PM line exhibits a minimum value of 0.2 kOe and diverges to lower temperature. To high temperatures the PM linewidth increases approximately with linear slope indicating relaxation via spin–phonon coupling [68], whereas linewidth of the FMR slightly increases with temperature and then decreases on approaching T_G. Thus the ESR results support the

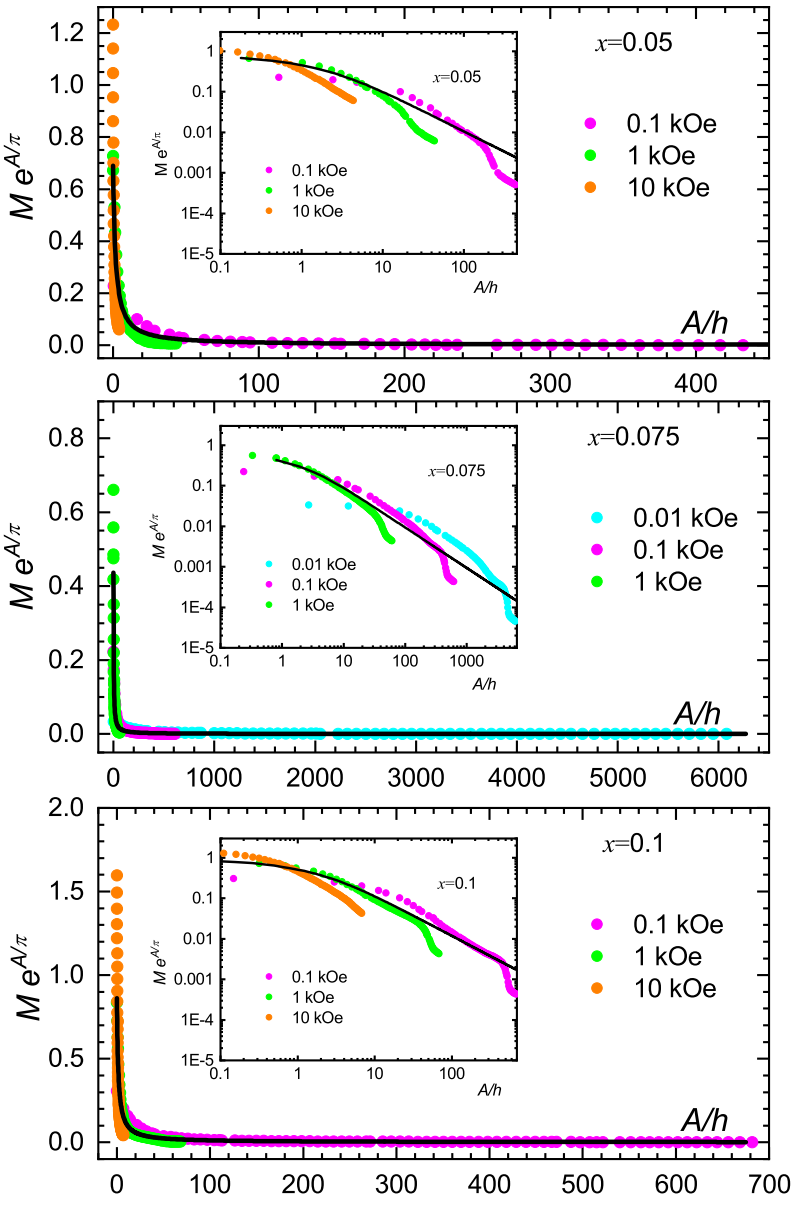

Fig. 7. Verification of the magnetization scaling behavior (black solid line) for $La_{0.7}Sr_{0.3}Mn_{0.9}Fe_{0.1-x}Zn_xO_3$ at different magnetic fields: for $x = 0.05$ and 0.1: $H = 100$ Oe (magenta), $H = 1$ kOe (green) and $H = 10$ kOe (orange); for $x = 0.075$: $H = 10$ Oe (cyan), $H = 100$ Oe (green), $H = 1$ kOe (orange). The inserts show the data on logarithmic scale.

findings of the magnetization measurements, i.e. the formation of FM clusters in the paramagnetic matrix in a certain temperature range above T_C limited by a common upper T_G characteristic of a Griffiths phase.

3.3. Magnetocaloric effect

To study the magnetocaloric effect, Fig. 10 shows the isothermal magnetization plots for x=0.05, 0.075, and 0.1 in the magnetic field range up to 50 kOe at several temperatures below and above T_C with temperature steps $\Delta T = 10$ K. The magnetic entropy change $-\Delta S_M$ can be calculated by

$$\Delta S_M(T,H) \sim \sum_i \frac{Mi - M_{i+1}}{T_{i+1} - T_i} \Delta H_i \quad (5)$$

where M_{i+1} and M_i are the values of magnetization at T_{i+1}, and T_i respectively, under a magnetic field H_i [17,19,69,70].

Based on Eq. (5), we calculated the values of $-\Delta S_M$ of all compounds, and the results are shown in Fig. 11. One can clearly see that at a certain value of field, $|\Delta S_M|$ reaches a maximum at a temperature close to T_C. Below 50 kOe, the values of $|\Delta S_M^{max}|$ are found to be 2.9, 2.6, and 2.68 J/kgK for $x = 0.05$, 0.075, and 0.1, respectively. Fig. 12a shows the maximum of the absolute value of the magnetic entropy change $|\Delta S_M^{max}|$ as a function of the change ΔH (not to be confused with the ESR linewidth) in the applied magnetic field from 10 to 50 kOe for all samples. The magnitude of the maximum of the magnetic entropy changes increases with increasing magnetic field change ΔH and attains its highest values near the magnetic phase-transition temperatures (T_C).

It is know that in addition to $|\Delta S_M|$, another important parameter in the practical design of magnetic refrigerants is the relative cooling power which is usually used to estimate the magnetic cooling efficiency of a magnetic material [71–73]. Based on the values of $|\Delta S_M|$, the relative cooling power (RCP) can be defined by

$$RCP = |\Delta S_M^{max}| \cdot \Delta T_{FWHM} \quad (6)$$

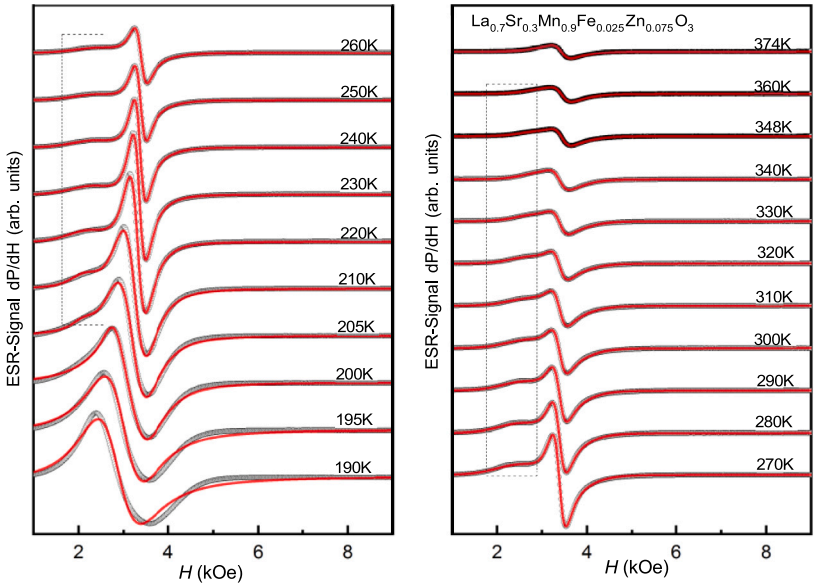

Fig. 8. ESR spectra of $La_{0.7}Sr_{0.3}Mn_{0.9}Fe_{0.025}Zn_{0.075}O_3$ at temperatures $190 \le T \le 374$ K. The red solid lines indicate fits with the field derivative of two Lorentz curves.

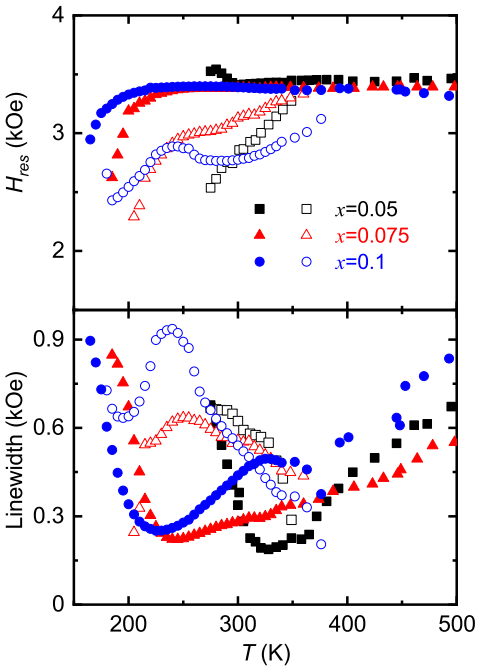

Fig. 9. Temperature dependence of the resonance fields H_{res} and linewidths in $La_{0.7}Sr_{0.3}Mn_{0.9}Fe_{0.1-x}Zn_xO_3$ (x=0.05, 0.075 and 0.1). Solid symbols: paramagnetic resonance, open symbols: ferromagnetic resonance.

where ΔT_{FWHM} is the full-width at half-maximum of the $-\Delta S_M$ curve [17,19,74–76]. The magnetic field change dependences of ΔT_{FWHM} and RCP are shown in Fig. 12(b, c), respectively. Accordingly, below ΔH= 50 kOe, the values of RCP are found to vary between 0.25 and 0.31 kJ/kg. As illustrated in Fig. 12c, there is an almost linear increase in the RCP values as the change in the applied magnetic field increases for all compounds with x = 0.075 having the largest RCP values compared to the other two compounds.

Note, that $|\Delta S_M^{max}|$ values for our compounds are lower than the $|\Delta S_M^{max}|$ values obtained for the compound $La_{0.7}Sr_{0.3}MnO_3$ at 50 kOe, while the RCP value for our samples is higher [77]. The magnitude of $|\Delta S_M^{max}|$ at the FM Curie temperature (at 50 kOe) and RCP in $La_{0.7}Sr_{0.3}MnO_3$ are 4.56 J/(kgK) and 128 J/kg, respectively [77].

Finally, we put our results into the context of existing reports on related compounds. Previous magnetic studies have shown that poly- and nano-crystalline samples of $La_{0.6}Sr_{0.4}Mn_{1-x}Fe_xO_3$ ($0 \le x \le 0.3$) [37], $La_{0.67}Sr_{0.33}Mn_{1-x}Fe_xO_3$ ($0 \le x \le 0.15$) [39], $La_{0.7}Sr_{0.3}Mn_{1-x}Fe_xO_3$ ($0.05 \le x \le 0.2$) [36,38,78] and $La_{0.8}Sr_{0.2}Mn_{1-x}Fe_xO_3$ ($0 \le x \le 0.15$) [40] with rhombohedral crystal structure (space group $R\bar{3}c$) undergo a ferromagnetic phase transition with magnetic entropy changes and RCP values comparable to our present data, e.g. $La_{0.7}Sr_{0.3}Mn_{1-x}Fe_xO_3$ with RCP =250 J/kg, $|\Delta S_M^{max}|$ = 4.4 J/kgK - x = 0.05; RCP = 168 J/kg, $|\Delta S_M^{max}|$ = 1.3 J/kgK - x = 0.2 [79]. It should also be noted that for some nanocrystalline samples of $La_{0.7}Sr_{0.3}Mn_{1-x}Fe_xO_3$ (x = 0.08–0.16), features characteristic of the Griffiths phase are visible in the temperature dependence of the inverse magnetic susceptibility [36]. For example, magnetic studies carried out for the nanocrystalline sample $La_{0.7}Sr_{0.3}Mn_{0.95}Fe_{0.05}O_3$ (T_C = 290 K, $|\Delta S_M^{max}|$ = 2.26 J/kgK at 3T) quite clearly indicate the presence of the Griffiths phase (T_G = 345 K) [38]. There is only one article in which the results of v-ray diffraction analysis indicate that the polycrystalline sample has an orthorhombic crystal structure (space group $Pnma$) [80]. Nevertheless, magnetic studies have shown that also this compound with orthorhombic crystal structure undergoes an FM–PM transition at T_C = 311 K with RCP = 127.9 J/kg, $|\Delta S_M^{max}|$ = 2.13 J/kgK [80].

4. Conclusions

Mössbauer measurements show that in the studied ferromagnetic perovskite-like manganites, doping with iron ions leads to the replacement of Mn^{3+} ions by Fe^{3+} ions in the high-spin state with the same ionic radius. It was found that on application of a magnetic field the maximum value of the magnetic entropy change at the FM–PM transition increases with Fe content reaching 2.9 J/(kgK) at a magnetic field change of 50 kOe for x = 0.05. The corresponding RCP values were found to be 0.258, 0.31 and 0.292 kJ/kg for the samples with x = 0.05, 0.075, and 0.1, respectively. With $T_C(x = 0.05)$ = 278 K, i.e. close to room temperature, this material is interesting for application in alternative refrigerator technology.

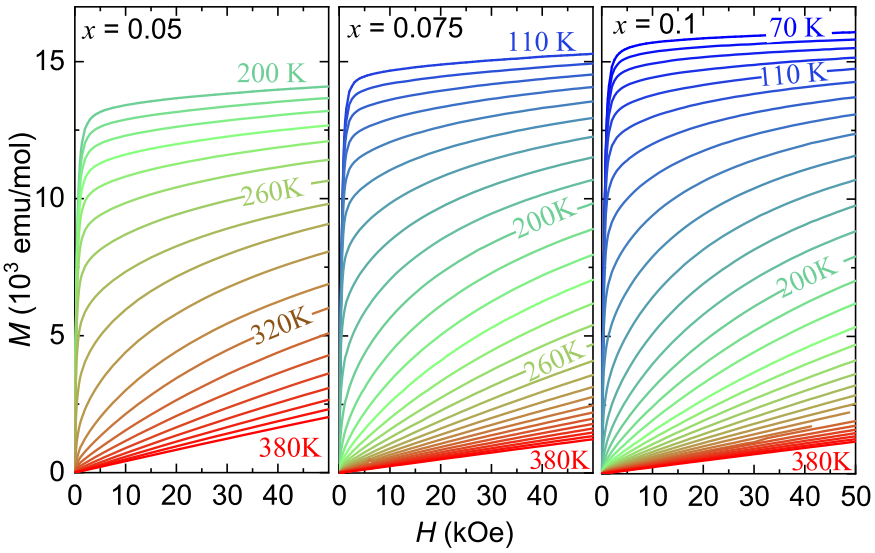

Fig. 10. Isothermal magnetization dependent on magnetic field in temperature steps of 10 K for $La_{0.7}Sr_{0.3}Mn_{0.9}Fe_{0.1-x}Zn_xO_3$ (x=0.05, 0.075, and 0.1).

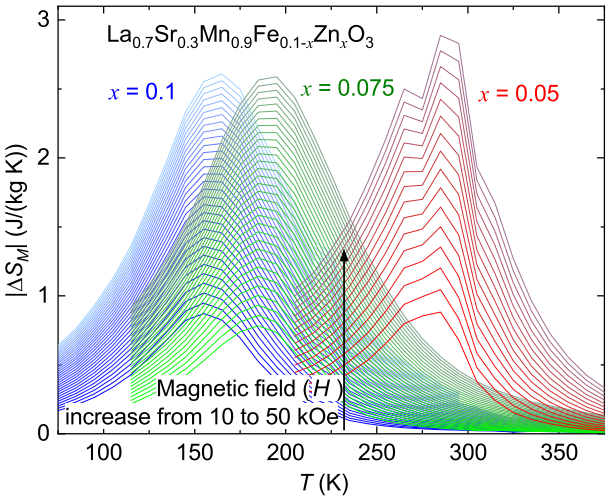

Fig. 11. Magnetic entropy change $|\Delta S_M(T)|$ curves corresponding to magnetic field changes ΔH = 10–50 kOe.

The Griffiths phase due to short-range order persists in the temperature region $T_C \leq T \leq T_G$. In this temperature range the inverse magnetic susceptibility of all compounds under investigation does not follow the CW law, which is ascribed to the presence of ferromagnetic clusters and satisfies the Griffiths model: in this respect the magnetization behavior above T_C for our compounds was theoretical analyzed using the scaling law derived from the Lee–Yang zeros distribution theory. This analysis enabled us to unequivocally identify the Griffiths phase behavior in all three compounds. Concomitantly, the FMR line coexisting with the PM ESR signal also corroborates that the GP model is appropriate to describe the short-range ordered state for x = 0.05, 0.075, and 0.1.

CRediT authorship contribution statement

Z.Y. Seidov: Writing – original draft, Supervision, Methodology, Investigation, Funding acquisition, Formal analysis, Data curation, Conceptualization. **I.V. Yatsyk:** Visualization, Methodology, Investigation, Formal analysis, Data curation. **A.V. Shestakov:** Visualization, Methodology, Investigation, Formal analysis, Data curation. **A.S. Ovchinnikov:** Writing – original draft, Visualization, Methodology, Investigation, Formal analysis, Data curation. **F.G. Vagizov:** Writing – original draft, Methodology, Investigation, Formal analysis, Data curation. **V.A. Shustov:** Methodology, Investigation, Formal analysis. **A.G. Badelin:** Methodology, Investigation, Formal analysis. **V.K. Karpasyuk:** Supervision, Resources, Methodology, Investigation, Formal analysis. **M.J. Najafzade:** Visualization, Resources, Investigation, Funding acquisition. **I.N. Ibrahimov:** Visualization, Resources, Investigation. **H.-A. Krug von Nidda:** Writing – review & editing, Supervision, Project administration, Investigation, Funding acquisition, Data curation, Conceptualization. **R.M. Eremina:** Writing – original draft, Supervision, Project administration, Methodology, Investigation, Funding acquisition, Formal analysis, Data curation, Conceptualization.

Declaration of competing interest

The authors declare that they have no known competing financial interests or personal relationships that could have appeared to influence the work reported in this paper.

Acknowledgments

The authors thank Dana Vieweg for SQUID measurements. This work was partially supported by the Deutsche Forschungsgemeinschaft (DFG) within the Transregional Collaborative Research Center TRR 360 “Constrained Quantum Matter”, project no. 492547816 (Augsburg, Munich, Stuttgart, Lepzig). Electron spin resonance and X-ray investigations (I.V. Yatsyk, V.A. Shustov, R.M. Eremina) were performed with the financial support from the government assignment for FRC Kazan Scientific Center of RAS. The work of Z.Y. Seidov, M.J. Najafzade and I.N. Ibrahimov was partially supported by the Science Development Foundation under the President of the Republic Azerbaijan Grant EIF-BGM-4-RFTF-1/2017-21/03/1-M-03. The work of A.V. Shestakov was financially supported by the government assignment for Prokhorov General Physics Institute of RAS. A.S. Ovchinnikov acknowledges the Ministry of Science and Higher Education of the Russian Federation (Ural Federal University Program of Development within the Priority-2030 Program).

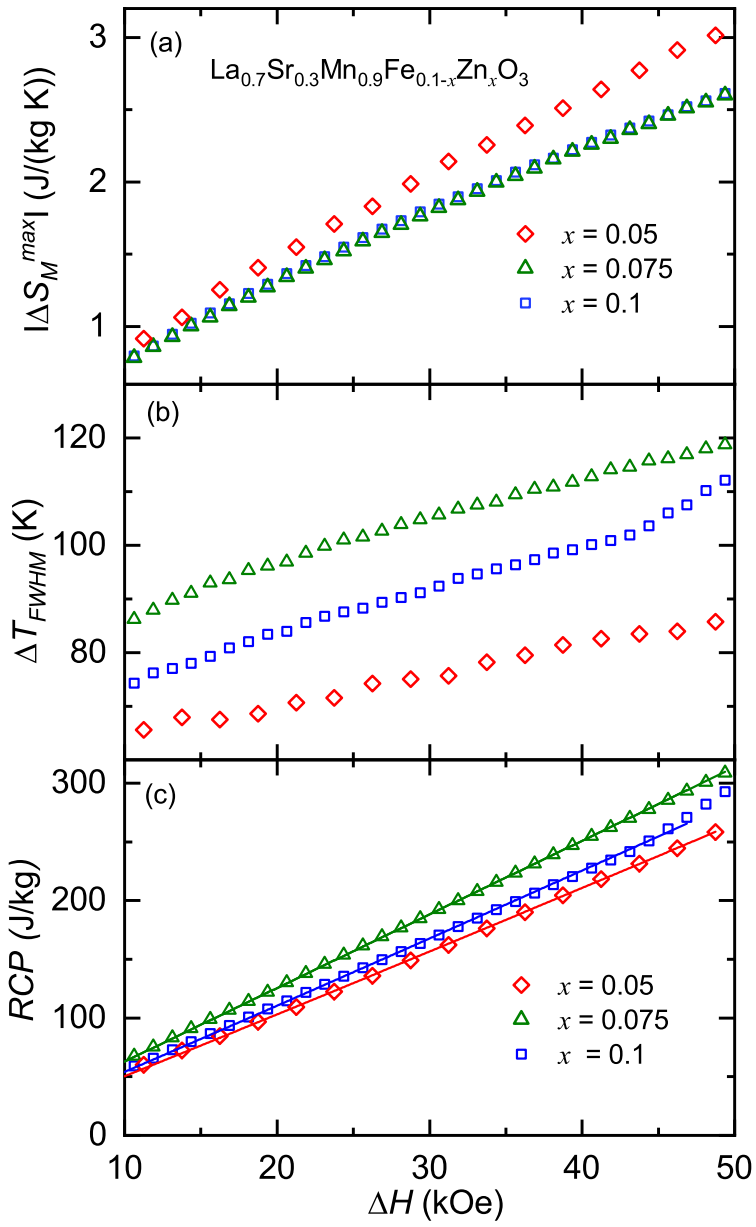

Fig. 12. $|\Delta S_M^{max}|$ (a), ΔT_{FWHM} (b) and relative cooling power (c) versus ΔH for $La_{0.7}Sr_{0.3}Mn_{0.9}Fe_{0.1-x}Zn_xO_3$ (x=0.05, 0.075, and 0.1). (c) Herein, the solid lines are the linear fitting curves of the RCP data.

References

[1] J.M.D. Coey, M. Viret, S. von Molnar, Mixed-valence manganites, Adv. Phys. 48 (2) (1999) 167, http://dx.doi.org/10.1080/000187399243455.

[2] E.L. Nagaev, Lanthanum manganites and other giant-magnetoresistance magnetic conductors, Phys.-Usp. 39 (8) (1996) 781, http://dx.doi.org/10.1070/PU1996v039n08ABEH000161.

[3] P. Schiffer, A.P. Ramirez, W. Bao, S.W. Cheong, Low temperature magnetoresistance and the magnetic phase diagram of $La_{1-x}Ca_xMnO_3$, Phys. Rev. Lett. 75 (18) (1995) 3336, http://dx.doi.org/10.1103/PhysRevLett.75.3336.

[4] C.N.R. Rao, A. Arulraj, Giant magnetoresistance, charge-ordering and related aspects of manganase oxides, Curr. Opin. Solid State Mater. Sci. 3 (1) (1998) 23, http://dx.doi.org/10.1016/S1359-0286(98)80061-2.

[5] A. Moreo, S. Yunoki, E. Dagotto, Phase separation scenario for manganese oxides and related materials, Science 283 (1999) 2034, http://dx.doi.org/10.1126/science.283.5410.2034.

[6] N.G. Bebenin, R.I. Zainullina, V. Ustinov, Colossal magnetoresistance manganites, Phys.-Usp. 61 (8) (2018) 719, http://dx.doi.org/10.3367/UFNe.2017.07.038180.

[7] J. Hemberger, A. Krimmel, T. Kurz, H.-A. Krug von Nidda, V.Yu. Ivanov, A.A. Mukhin, A.M. Balbashov, A. Loidl, Structural, magnetic, and electrical properties of single-crystalline $La_{1-x}Sr_xMnO_3$ ($0.4 \leq x \leq 0.85$), Phys. Rev. B 66 (9) (2002) 094410, http://dx.doi.org/10.1103/PhysRevB.66.094410.

[8] J.-S. Zhou, J.B. Goodenough, Local structural distortions, orbital ordering, and ferromagnetism in underdoped $La_{1-x}Sr_xMnO_3$, Phys. Rev. B 91 (6) (2015) 064414, http://dx.doi.org/10.1103/PhysRevB.91.064414.

[9] E. Dagotto, T. Hotta, A. Moreo, Colossal magnetoresistant materials: the key role of phase separation, Phys. Rep. 344 (1–3) (2001) 1–153, http://dx.doi.org/10.1016/S0370-1573(00)00121-6.

[10] V.N. Krivoruchko, The Griffiths phase and the metal-insulator transition in substituted manganites, Low Temp. Phys. 40 (7) (2014) 586, http://dx.doi.org/10.1063/1.4890365.

[11] C. Zener, Interaction between the d-shells in the transition metals. II. Ferromagnetic compounds of manganese with perovskite structure, Phys. Rev. 82 (3) (1951) 403, http://dx.doi.org/10.1103/PhysRev.82.403.

[12] E.O. Wollan, W.C. Koehler, Neutron diffraction study of the magnetic properties of the series of perovskite-type compounds $La_{1-x}Ca_xMnO_3$, Phys. Rev. 100 (2) (1955) 545, http://dx.doi.org/10.1103/PhysRev.100.545.

[13] Y. Zhang, Y. Xie, J. Wei, W. Hao, Experimental and theoretical insights into the structural, magnetic, and low-temperature magnetocaloric properties of RE_2CoTiO_6 (RE=Gd, Dy, and Er) double perovskite oxides, J. Mater. Chem. A 12 (2024) 32396–32407, http://dx.doi.org/10.1039/D4TA05172F.

[14] R. Ji, Y. Du, X. Na, X. Wang, L. Li, Investigation of the structural and cryogenic magnetic properties in Gd_2CrCoO_6 oxide, Inorg. Chem. Commun. 174 (1) (2025) 113964, http://dx.doi.org/10.1016/j.inoche.2025.113964.

[15] Y. Zhang, Y. Na, W. Hao, T. Gottschall, L. Li, Enhanced cryogenic magnetocaloric effect from 4f-3d exchange interaction in B-site ordered Gd_2CuTiO_6 double perovskite oxide, Adv. Funct. Mater. 34 (49) (2024) 2409061, http://dx.doi.org/10.1002/adfm.202409061.

[16] W. Hao, R. Ji, L. Zhu, S. Huang, Y. Zhang, Structural, magnetic and cryogenic magnetocaloric properties in Gd_2CrFeO_6 ceramic oxide, Solid State Commun. 339 (2025) 115876, http://dx.doi.org/10.1016/j.ssc.2025.115876.

[17] T.M. Al Shahumi, I.A. Al Omari, S.H. Al Harthi, M.T. Zar Myint, Synthesis, structure, morphology, magnetism, and magnetocaloric-effect studies of $(La_{1-x}Pr_x)_{0.7}Sr_{0.3}MnO_3$ nanocrystalline perovskites, SN Appl. Sci. 5 (2023) 121, http://dx.doi.org/10.1007/s42452-023-05328-5.

[18] A. Tozri, J. Khelifi, E. Dhahri, E.K. Hlil, Influence of Pr doping on magnetic phase transition and magnetocaloric effect of $La_{0.7-x}Pr_xBa_{0.3}MnO_3$ manganite, Mater. Chem. Phys. 149–150 (2015) 728–733, http://dx.doi.org/10.1016/j.matchemphys.2014.11.034.

[19] D.C. Linh, N.T.V. Chinh, N.T. Dung, L.V. Bau, N.H. Duc, D.H. Mahn, T.D. Thanh, Critical behavior and room temperature magnetocaloric effect of La-doped $Pr_{0.7}Sr_{0.3}MnO_3$ compounds, Phys. B 661 (2023) 414945, http://dx.doi.org/10.1016/j.physb.2023.414945.

[20] V. Franco, J.S. Blazquez, J.J. Ipus, J.Y. Law, L.M. Moreno-Ramirez, A. Conde, Magnetocaloric effect: From materials research to refrigeration devices, Prog. Mater. Sci. 93 (2018) 112–232, http://dx.doi.org/10.1016/j.pmatsci.2017.10.005.

[21] A.M. Aliev, A.G. Gamzatov, Magnetocaloric effect in manganites in alternating magnetic fields, J. Magn. Magn. Mater. 553 (2022) 169300, http://dx.doi.org/10.1016/j.jmmm.2022.169300.

[22] V.E. Salazar-Munoz, A. Lobo Guerrero, S.A. Palomares-Sanchez, Review of magnetocaloric properties in lanthanum manganites, J. Magn. Magn. Mater. 562 (2022) 169787, http://dx.doi.org/10.1016/j.jmmm.2022.169787.

[23] A.O. Ayas, S.K. Çetin, G. Akça, M. Akyol, A. Ekicibil, Magnetic refrigeration: Current progress in magnetocaloric properties of perovskite manganite materials, Mater. Today Commun. 35 (2023) 105988, http://dx.doi.org/10.1016/j.mtcomm.2023.105988.

[24] K.A. Gschneidner, Jr., V.K. Pecharsky, Thirty years of near room temperature magnetic cooling: Where we are today and future prospects, Int. J. Refrig. 31 (6) (2008) 945–961, http://dx.doi.org/10.1016/j.ijrefrig.2008.01.004.

[25] B. Dorin, J. Avsec, A. Plesca, The efficiency of magnetic refrigeration and a comparison with compresor refrigeration systems, J. Energy Tecnol. 11 (3) (2018) 59–69, doi:fe.um.si/images/jet/JET-november-2018-splet-5.pdf.

[26] Z.Y. Seidov, I.V. Yatsyk, F.G. Vagizov, V.A. Shustov, A.G. Badelin, V.K. Karpasyuk, M.J. Najafzade, I.N. Ibrahimov, S.Kh. Estemirova, H.-A. Krug von Nidda, R.M. Eremina, Local magnetic properties of $La_{0.83}Sr_{0.17}Mn_{0.9}Fe_{0.1-x}Zn_xO_3$, J. Magn. Magn. Mater. 552 (18) (2022) 169190, http://dx.doi.org/10.1016/j.jmmm.2022.169190.

[27] R.B. Griffiths, Nonanalytic behavior above the critical point in a random ising ferromagnet, Phys. Rev. Lett. 23 (1) (1969) 17–19, http://dx.doi.org/10.1103/PhysRevLett.23.17.

[28] V.M. Galitski, A. Kaminski, S.D. Sarma, Griffiths phase in diluted magnetic semiconductors, Phys. Rev. Lett. 92 (17) (2004) 177203, http://dx.doi.org/10.1103/PhysRevLett.92.177203.

[29] W. Jiang, X. Zhou, G. Williams, Y. Mukovskii, K. Glazyrin, Griffiths phase and critical behavior in single-crystal $La_{0.7}Ba_{0.3}MnO_3$: Phase diagram for $La_{1-x}Ba_xMnO_3$ ($x \leq 0.33$), Phys. Rev. B 77 (6) (2008) 064424, http://dx.doi.org/10.1103/PhysRevB.77.064424.

[30] S. Zhou, Y. Guo, J. Zhao, L. He, L. Shi, Size-induced Griffiths phase and second-order ferromagnetic transition in $Sm_{0.5}Sr_{0.5}MnO_3$ nanoparticles, J. Phys. Chem. C 115 (5) (2011) 1535, http://dx.doi.org/10.1021/jp108553r.

[31] J. Mizusaki, N. Mori, H. Takai, Y. Yonemura, H. Minamiue, H. Tagawa, M. Dokiya, H. Inaba, K. Naraya, T. Sasamoto, T. Hashimoto, Oxygen nonstoichiometry and defect equilibrium in the perovskite-type oxides $La_{1-x}Sr_xMnO_{3+d}$, Solid State Ion. 129 (1–4) (2000) 163–177, http://dx.doi.org/10.1016/S0167-2738(99)00323-9.

[32] B. Uthaman, A. Prasad, M. Hariram, Structural analysis of $La_{0.7}Sr_{0.3}MnO_3$ manganite synthesized by sol-gel and solid-state route, IOP Conf. Ser.: Mater. Sci. Eng. 1263 (2022) 012036, http://dx.doi.org/10.1088/1757-899X/1263/1/012036.

[33] S. Keshri, S. Rajput, S. Biswas, L. Joshi, W. Suski, P. Wisniweski, Structural, magnetic and transport properties of Ca and Sr doped lanthanum manganites, J. Met. Mater. Miner. 31 (4) (2021) 62–68, http://dx.doi.org/10.14456/jmmm.2021.58.

[34] D.H. Manh, T.T.N. Nha, L.T.H. Phong, P.H. Nam, T.D. Thanh, P.T. Phong, Determination of the crystalline size of hexagonal $La_{1-x}Sr_xMnO_3$ (x=0.3) nanoparticles from X-ray diffraction – a comparative study, RSC Adv. 13 (2023) 25007, http://dx.doi.org/10.1039/d3ra04018f.

[35] N. Kemik, Y. Takamura, A. Navrotsky, Thermochemistry of $La_{0.7}Sr_{0.3}Mn_{1-x}Fe_xO_3$ solid solutions ($0 \leq x \leq 1$), J. Solid State Chem. 184 (4) (2011) 2118–2123, http://dx.doi.org/10.1016/j.jssc.2011.05.039.

[36] T.M. Al-Sashumi, I.A. Al-Omari, S.H. Al-Harthi, M.T.Z. Myint, P. Kharel, S. Lamichhane, S-H. Liou, Synthesis, structure, morphology, magnetism, and magnetocaloric-effect studies of $La_{0.7}Sr_{0.3}Mn_{1-x}Fe_xO_3$ perovskite nanoparticles, J. Alloys Compd. 958 (2023) 170454, http://dx.doi.org/10.1016/j.jallcom.2023.170454.

[37] J.J. Qian, W.H. Qi, Z.Z. Li, L. Ma, G.D. Tang, Y.N. Du, M.Y. Chen, G.H. Wu, F.X. Hu, Spin-dependent and spin-independent channels of electrical transport in perovskite manganites, RSC Adv. 8 (2018) 4417, http://dx.doi.org/10.1039/c7ra12878a.

[38] T.D. Thanh, N.V. Quynh, T.T.N. Nha, P.H. Nam, D.H. Manh, P.T. Phong, Correlation between critical magnetic behavior and grif!ths phase in ferromagnetic $La_{0.7}Sr_{0.3}Mn_{1-x}Fe_xO_3$ (x= 0.05) nanoparticle, Phys. Scr. 98 (2023) 105533, http://dx.doi.org/10.1088/1402-4896/acfb4c.

[39] Y. Zhou, X. Zhu, S. Li., Structure, magnetic, electrical transport and magnetoresistance properties of $La_{0.67}Sr_{0.33}Mn_{1-x}Fe_xO_3$ ($0 \leq x \leq 0.15$), doped manganite coatings, Ceram. Int. 43 (4) (2017) 3679–3687, http://dx.doi.org/10.1016/j.ceramint.2016.11.210.

[40] S.Kh. Estemirova, V.Ya. Mitrofanov, S.A. Uporov, G.A. Kozhina, Fe substitution for Mn in rhombohedral $La_{0.8}Sr_{0.2}Mn_{1-x}Fe_xO_3$ — the structural magnetic, and magnetocaloric properties, J. Supercond. Nov. Magn. 35 (2022) 1251–1259, http://dx.doi.org/10.1007/s10948-022-06188-7.

[41] Maud, Materials analysis using diffraction, http://maud.radiographema.eu.

[42] D.V. Popov, T.P. Gavrilova, I.F. Gilmutdinov, M.A. Cherosov, V.A. Shustov, E.M. Moshkina, L.N. Bezmaternykh, R.M. Eremina, Magnetic properties of ludwigite $Mn_{2.25}Co_{0.75}BO_5$, J. Phys. Chem. Solids 148 (2021) 109695, http://dx.doi.org/10.1016/j.jpcs.2020.109695.

[43] M.E. Matsnev, V.S. Rusakov, SpectrRelax: An application for Mössbauer spectra modeling and fitting, AIP Conf. Proc. 1489 (1) (2012) 178–185, http://dx.doi.org/10.1063/1.4759488.

[44] R.M. Eremina, I.V. Yatsyk, Z.Y. Seidov, F.G. Vagizov, V.A. Shustov, A.G. Badelin, V.K. Karpasyuk, D.S. Abdinov, M.M. Tagiev, S.Kh. Estemirova, H.-A. Krug von Nidda, Magnetic properties of $La_{0.81}Sr_{0.19}Mn_{0.9}Fe_{0.1-x}Zn_xO_3$ x=0 and x=0.05, Appl. Magn. Reson. 54 (4–5) (2023) 449–461, http://dx.doi.org/10.1007/s00723-022-01510-x.

[45] F. Menil, Systematic trends of the ^{57}Fe Mössbauer isomer shifts in (FeO_n) and (FeF_n) polyhedral. Evidence of a new correlation between the isomer shift and the inductive effect of the competing bond T-X (-Fe) (where X is O or F and T any element with a formal positive charge), J. Phys. Chem. Solids 46 (7) (1985) 763–789, http://dx.doi.org/10.1016/0022-3697(85)90001-0.

[46] E. Murad, J. Cashion, Mössbauer Spectroscopy of Environmental Materials and their Industrial Utilization, Springer Science+Business Media, New York, 2004, p. 418, http://dx.doi.org/10.1007/978-1-4419-9040-2.

[47] K. De, R. Ray, R.N. Panda, S. Giri, H. Nakamura, T. Kohara, The effect of Fe substitution on magnetic and transport properties of $LaMnO_3$, J. Magn. Magn. Mater. 288 (2005) 339–346, http://dx.doi.org/10.1016/j.jmmm.2004.09.118.

[48] M. Pissas, G. Kallias, E. Devlin, A. Simopoulos, D. Niarchos, Mössbauer study of $La_{0.75}Ca_{0.25}Mn_{0.98}Fe_{0.02}O_3$ compound, J. Appl. Phys. 81 (1997) 5770–5772, http://dx.doi.org/10.1063/1.364722.

[49] A.G. Silva, K.L. Salcedo Rodriguez, C.P. Contreras Medrano, G.S G. Lourenco, M. Boldrin, E. Baggio-Saitovitch, L. Bufaical, Griffiths phase and spontaneous exchange bias in $La_{1.5}Sr_{0.5}CoMn_{0.5}Fe_{0.5}O_6$, J. Phys.: Condens. Matter. 33 (6) (2021) 065804, http://dx.doi.org/10.1088/1361-648X/abc595.

[50] S. Thota, S. Ghosh, Maruthi R, D.C. Joshi, R. Medwal, R.S. Rawat, M.S. Seehra, Magnetic ground state and exchange interactions in the ising chain ferromagnet $CoNb_2O_6$, Phys. Rev. B 103 (6) (2021) 064415, http://dx.doi.org/10.1103/PhysRevB.103.064415.

[51] J. Deisenhofer, D. Braak, H.-A. Krug von Nidda, J. Hemberger, R.M. Eremina, V.A. Ivanshin, A.M. Balbashov, G. Jug, A. Loidl, T. Kimura, Y. Tokura, Observation of a Griffiths phase in paramagnetic $La_{1-x}Sr_xMnO_3$, Phys. Rev. Lett. 95 (12) (2005) 257202, http://dx.doi.org/10.1103/PhysRevLett.95.257202.

[52] N. Rama, M.S. Ramachandra Rao, V. Sankaranarayanan, P. Majewski, S. Gepraegs, M. Opel, R. Gross, A-site-disorder-dependent percolative transport and Griffiths phase in doped manganites, Phys. Rev. B 70 (22) (2004) 224424, http://dx.doi.org/10.1103/PhysRevB.70.224424.

[53] X. Zheng, T. Gao, W. Jing, X. Wang, Y. Liu, B. Chen, H. Dong, Z. Chen, S. Cao, C. Cai, V.V. Marchenkov, Evolution of Griffiths phase and spin reorientation in perovskite manganites, J. Magn. Magn. Mater. 491 (1) (2019) 165611, http://dx.doi.org/10.1016/j.jmmm.2019.165611.

[54] M.B. Salamon, P. Lin, S.H. Chun, Colossal magnetoresistance is a Griffiths singularity, Phys. Rev. Lett. 88 (19) (2002) 197203, http://dx.doi.org/10.1103/PhysRevLett.88.197203.

[55] M.B. Salamon, S.H. Chun, Griffiths singularities and magnetoresistive manganites, Phys. Rev. B 68 (1) (2003) 014411, http://dx.doi.org/10.1103/PhysRevB.68.014411.

[56] A.K. Pramanik, A. Banerjee, Griffiths phase and its evolution with Mn-site disorder in the half-doped manganite $Pr_{0.5}Sr_{0.5}Mn_{1-y}Ga_yO_3$ (y=0.0, 0.025, and 0.05), Phys. Rev. B 81 (2) (2010) 024431, http://dx.doi.org/10.1103/PhysRevB.81.024431.

[57] R.M. Eremina, I.I. Fazlizhanov, I.V. Yatsyk, K.R. Sharipov, A.V. Pyataev, H.-A. Krug von Nidda, N. Pascher, A. Loidl, K.V. Glazyrin, Ya.M. Mukovskii, Phase separation in paramagnetic $Eu_{0.6}La_{0.4-x}Sr_xMnO_3$, Phys. Rev. B 84 (6) (2011) 064410, http://dx.doi.org/10.1103/PhysRevB.84.064410.

[58] Pak Yuen Chan, Nigel Goldenfeld, Myron Salamon, Critical behavior of Griffiths ferromagnets, Phys. Rev. Lett. 97 (13) (2006) 137201, http://dx.doi.org/10.1103/PhysRevLett.97.137201.

[59] A.J. Bray, D. Huifang, Griffiths singularities in random magnets: Results for a soluble model, Phys. Rev. B 40 (10) (1989) 6980–6986, http://dx.doi.org/10.1103/PhysRevB.40.6980.

[60] A.J. Bray, Nature of the Griffiths phase, Phys. Rev. Lett. 59 (5) (1987) 586–589, http://dx.doi.org/10.1103/PhysRevLett.59.586.

[61] C.N. Yang, T.D. Lee, Statistical theory of equations of state and phase transitions. I. Theory of condensation, Phys. Rev. 87 (3) (1952) 404–409, http://dx.doi.org/10.1103/PhysRev.87.404.

[62] T.D. Lee, C.N. Yang, Statistical theory of equations of state and phase transitions. II. Lattice gas and ising model, Phys. Rev. 87 (3) (1952) 410–419, http://dx.doi.org/10.1103/PhysRev.87.410.

[63] A.S. Ovchinnikov, J.G. Ruziev, N.M. Nosova, E.M. Sherokalova, N.V. Selezneva, N.V. Baranov, Unbiased identification of the Griffiths phase in intercalated transition metal dichalcogenides by using Lee-Yang zeros, Phys. Rev. B 106 (2) (2022) L020401, http://dx.doi.org/10.1103/PhysRevB.106.L020401.

[64] S.I. Andronenko, A.A. Rodionov, A.V. Fedorova, S.K. Misra, Electron paramagnetic resonance study of $(La_{0.33}Sm_{0.67})_{0.67}Sr_{0.33-x}Ba_xMnO_3$ ($x < 0.1$): Griffiths phase, J. Magn. Magn. Mater. 326 (2013) 151–156, http://dx.doi.org/10.1016/j.jmmm.2012.08.017.

[65] A.S. Kumar, R. Reddy K, A.K. Bhatnagar, Magnetization and ESR studies of $La_{0.67}(Ca_{1-x}Mg_x)_{0.33}MnO_3$ systems, J. Alloys Compd. 639 (2015) 139–144, http://dx.doi.org/10.1016/j.jallcom.2015.03.028.

[66] R.M. Eremina, I.V. Yatsyk, Ya.M. Mukovskii, H.-A. Krug von Nidda, A. Loidl, Determination of the region of existence of ferromagnetic nanostructures in the paraphase of $La_{1-x}Ba_xMnO_3$ by the EPR method, JETP Lett. 85 (1) (2007) 51, http://dx.doi.org/10.1134/S0021364007010109.

[67] S.K. Misra, S.I. Andronenko, S. Asthana, D. Bahadur, A variable temperature EPR study of the manganites$(La_1/3Sm_{2/3})_{2/3}Sr_xBa_{0.33-x}MnO_3$ (x=0.0, 0.1, 0.2, 0.33): Small polaron hopping conductivity and Griffiths phase, J. Magn. Magn. Mater. 322 (19) (2010) 2902, http://dx.doi.org/10.1016/j.jmmm.2010.05.003.

[68] D.L. Huber, M.S. Seehra, Contribution of the spin-phonon interaction to the paramagnetic resonance linewidth of $CrBr_3$, J. Phys. Chem. Solids 36 (7–8) (1975) 723–725, http://dx.doi.org/10.1016/0022-3697(75)90094-3.

[69] V. Franco, Determination of the magnetic entropy change from magnetic measurements:the importance of the measurement protocol, LakeShore Cryotronics.

[70] W. Chen, Y. Na, F. Chen, Y. Zhang, Cryogenic magnetic and magnetocaloric properties in anhydrous rare-earth sulfate $RE_2(SO_4)_3$ (RE=Tb, Dy, Ho, Er), Cryogenics 146 (2025) 104012, http://dx.doi.org/10.1016/j.cryogenics.2024.104012.

[71] Y. Zhang, J.Y. Law, A. Li, W. Hao, V. Franco, L. Li, Unveiling the structural, electronic and magnetic properties of $Gd_{4.5}A_{0.5}Si_3O_{13}$ (A=K, Na, and Li) oxides with promising potential for low-temperature magnetic cooling, Small 21 (2025) 2409981, http://dx.doi.org/10.1002/smll.202409981.

[72] F. Chen, Y. Na, Y. Xie, Y. Zhang, Insight into the structural and magnetic properties of PrZnSi and NdZnSi compounds featuring large low-temperature magnetocaloric effects, ACS Appl. Mater. Interfaces 16 (39) (2025) 52719, http://dx.doi.org/10.1021/acsami.4c13601.

[73] M.E. Wood, W.H. Potter, General analysis of magnetic refrigeration and its optimization using a new concept: maximization of refrigerant capacity, Cryogenics 25 (12) (1985) 667, http://dx.doi.org/10.1016/0011-2275(85)90187-0.

[74] O. Tegus, E. Bruck, K.H.J. Buschow, F.R. de Boer, Transition-metal-based magnetic refrigerants for room-temperature applications, Nature 415 (2002) 150, http://dx.doi.org/10.1038/415150a.

[75] N.A. de Oliveira, P.J. von Ranke, Magnetocaloric effect around a magnetic phase transition, Phys. Rev. B 77 (2008) 214439, http://dx.doi.org/10.1103/PhysRevB.77.214439.

[76] K.A. Gschneidner, Jr., V.K. Pecharsky, Magnetocaloric materials, Annu. Rev. Mater. Res. 30 (1) (2000) 387–429, http://dx.doi.org/10.1146/annurev.matsci.30.1.387.

[77] S.K. Barik, R. Mahendiran, Effect of Bi doping on magnetic and magnetocaloric properties of $La_{0.7-x}Bi_xSr_{0.3}MnO_3$ ($0 \le x \le 0.4$), J. Appl. Phys. 107 (2010) 093906, http://dx.doi.org/10.1063/1.3407523.

[78] T. Hernandeza, F. Plazaola, T. Rojo, J.M. Barandiaran, Fe doping in $La_{0.7}Sr_{0.3}MnO_3$ magnetoresistant perovskite, J. Alloys Compd. 323–324 (2001) 440–443, http://dx.doi.org/10.1016/S0925-8388(01)01074-X.

[79] S.K. Barik, C. Krishnamoorthi, R. Mahendiran, Effect of Fe substitution on magnetocaloric effect in $La_{0.7}$ $Sr_{0.3}Mn_{1-x}Fe_xO_3$ ($0.05 \le x \le 0.2$), J. Magn. Magn. Mater. 323 (2011) 1015–1021, http://dx.doi.org/10.1016/j.jmmm.2010.12.007.

[80] I. Dhahri, M. Ellouze, T. Mnasri, E.K. Hlil, R.B. Jotania, Structural, magnetic, magnetocaloric and critical exponents of oxide manganite in $La_{0.7}Sr_{0.3}Mn_{0.95}Fe_{0.5}O_3$, J. Mater. Sci., Mater. Electron. 31 (2020) 12493–12501, http://dx.doi.org/10.1007/s10854-020-03797-7.